

# Evolution in Catalyst Morphology Leads to Carbon Nanotube Growth Termination

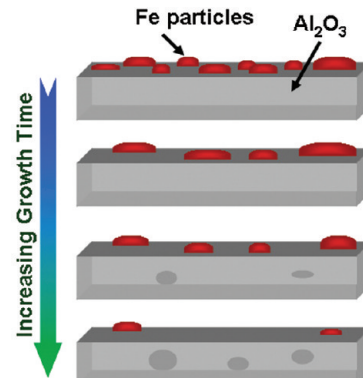
Seung Min Kim,<sup>†,#</sup> Cary L. Pint,<sup>§,#</sup> Placidus B. Amama,<sup>‡,⊥</sup> Dmitri N. Zakharov,<sup>†</sup>  
Robert H. Hauge,<sup>§</sup> Benji Maruyama,<sup>\*,†</sup> and Eric A. Stach<sup>\*,†</sup>

<sup>†</sup>School of Materials Engineering and Birck Nanotechnology Center, Purdue University, West Lafayette, Indiana 47907,

<sup>§</sup>Richard E. Smalley Institute for Nanoscale Science and Technology, Department of Physics and Astronomy, and Department of Chemistry, Rice University, Houston, Texas 77005, <sup>‡</sup>University of Dayton Research Institute, University of Dayton, Dayton, Ohio 45469, and <sup>¶</sup>Materials and Manufacturing Directorate, Air Force Research Laboratory, Wright-Patterson Air Force Base, Ohio 45433

**ABSTRACT** A mechanism by which catalyst deactivation occurs during vertically aligned single-walled carbon nanotube (SWNT) growth is demonstrated. We have used both quantitative measurements of nanotube growth rates and ex situ and in situ transmission electron microscopy observations to show that termination of carbon nanotube (CNT) array growth can be intrinsically linked to evolution of the catalyst morphology. Specifically, we find that a combination of both Ostwald ripening and subsequent subsurface diffusion leads to loss of the Fe catalyst, and through direct observations, we correlate this with nanotube growth termination. These observations indicate that careful design of the catalyst and its support – as well as the interaction between the two – is required to maximize nanotube yields.

## SECTION Nanoparticles and Nanostructures



Infinitely long carbon nanotubes (CNTs) are macroscopic 1-D quantum systems of incredible interest, and their creation is the goal of many research efforts. Progress toward this goal has resulted in enhanced catalyst lifetimes in aligned single-walled carbon nanotube (SWNT) growth through the addition of water vapor<sup>1–5</sup> or the use of a bimetallic catalyst such as Fe–Mo.<sup>6,7</sup> Rational approaches to engineering a catalyst to enhance its catalytic activity and lifetime for SWNT array growth are required to create structures that can exploit the remarkable electrical, thermal, and mechanical properties of long, continuous CNTs.<sup>8</sup> However, until the mechanism for catalyst deactivation is understood, approaches to combat the mortality of the catalyst in this growth process are likely to prove futile. As a result, the primary bottleneck in achieving multiple-meter-long CNTs is the lack of a coherent understanding of why growth termination occurs.

In vertically aligned SWNT growth, the metal catalyst layer consists of small (< 10 nm) islands or particles on a fixed oxide support layer. Vertical alignment is achieved as a result of the packing of particles, which constrains the collective growth of nanotubes in the direction perpendicular to the substrate. However, a surface-supported metal catalyst is not unique to SWNT array growth but is also utilized in the synthesis of a variety of other 1-D materials. For example, Hannon and co-workers<sup>9</sup> recently observed that Au nanodroplets that catalyze Si nanowires during vapor–liquid–solid (VLS) growth exhibit considerable atomic surface diffusion, which strongly impacts nanowire growth. In comparison to these observations of VLS nanowire growth, the catalysts producing SWNT arrays are packed closer and are

substantially smaller. Nonetheless, most current hypotheses for SWNT array termination assume either (i) a static catalyst layer where catalyst deactivation occurs from excess carbon (i.e., carbide formation, carbon overcoating, etc.)<sup>10–13</sup> or (ii) a mechanism that occurs independent of the catalyst layer, such as mechanical coupling of nanotubes in the array.<sup>14</sup> Alternatively, SWNT growth termination on SiO<sub>2</sub> is observed to occur through the formation of Fe silicides,<sup>15</sup> although this substrate does not support high-density SWNT array growth. Although these explanations may be important to growth termination, our recent work<sup>5,16</sup> has correlated the role of water vapor during growth to inhibition of Ostwald ripening, leading to enhanced catalyst lifetimes. Here, we explicitly demonstrate that both surface and subsurface migration of metal atoms leads to morphological changes in the catalyst particles (mass loss from individual catalysts) that correlate well with the time evolution and eventual termination of water-assisted SWNT growth.

Our experiments (described in more detail in the Supporting Information) were carried out in two growth systems, a water-assisted chemical vapor deposition (CVD) apparatus operating at 1.4 Torr (described elsewhere)<sup>4,17</sup> and an environmental cell transmission electron microscope (E-TEM) (80–300 S/TEM FEI Titan). For both, vertically aligned SWNTs grow from a catalyst supported by a thin alumina layer located underneath of the growing array (also known as

Received Date: December 30, 2009

Accepted Date: February 9, 2010

Published on Web Date: February 22, 2010

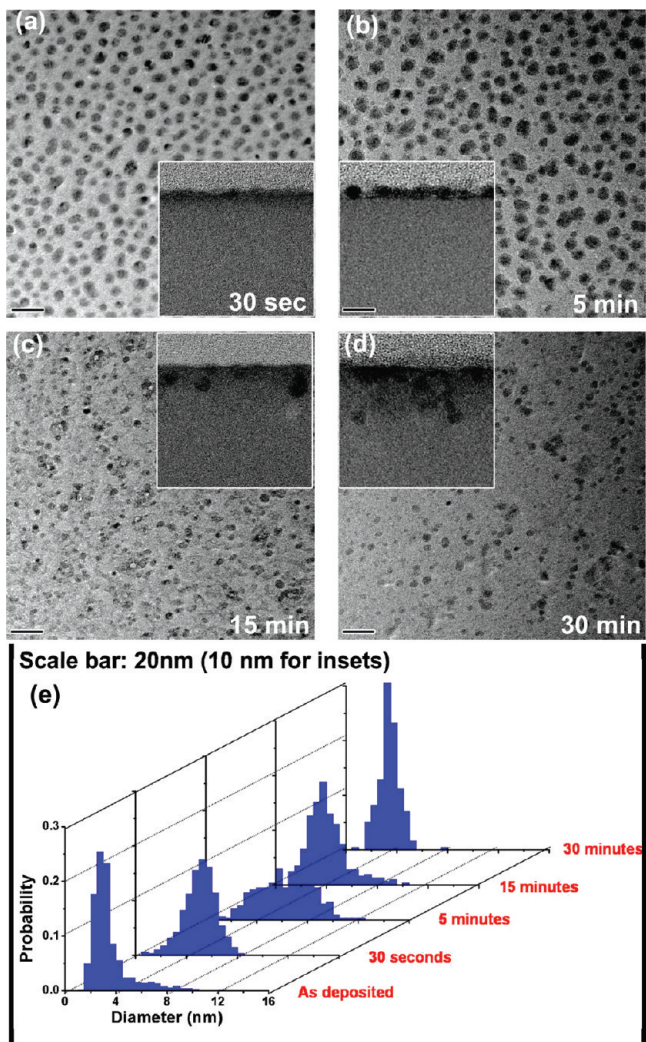


**Figure 1.** Plan-view TEM images of annealed Fe/Al<sub>2</sub>O<sub>3</sub> catalyst layers at 750 °C for various labeled times for (a) 30 s, (b) 5 min, (c) 15 min, and (d) 30 min. Insets are cross-sectional views demonstrating subsurface diffusion of Fe into the Al<sub>2</sub>O<sub>3</sub> layer. (e) Statistical representation of the catalyst particle size distribution for the four cases shown in (a)–(d) and the as-deposited Fe sample.

base or root growth), which leads us to characterize the time evolution of catalyst morphology using the same approach as our previous studies.<sup>5</sup> The catalyst samples consisted of an Fe layer (0.5 nm) evaporated onto an alumina support (10 or 100 nm) that was evaporated onto p-doped Si(100) with a native oxide. This catalyst/support combination is typically utilized in SWNT array growth,<sup>1,4,17,18</sup> resulting in a process in which the catalyst layer remains at the base of the growing SWNT array.<sup>19</sup>

As shown in Figure 1, TEM characterization of the catalyst layers following thermal annealing in ~1.5 Torr of H<sub>2</sub>/H<sub>2</sub>O (typical growth conditions without C<sub>2</sub>H<sub>2</sub>) at 750 °C as a function of time indicates the initial formation of particles having diameters consistent with that expected from the water-assisted SWNT growth process. In Figure 1, between 30 s and 5 min of annealing, evidence of Ostwald ripening is apparent,<sup>5,20</sup> based upon the emergence of larger particles

and a decreasing total number density of particles. Surprisingly, beyond 5 min of thermal annealing, the resulting particle size distribution can no longer be described by Ostwald ripening as both the overall particle size and the total number density of particles decrease. Longer annealing times further emphasize this trend, with a decreasing population of larger particles seen after 30 min. Cross-sectional TEM images of the same samples (insets to Figure 1) show that Fe diffuses into the alumina support layer, forming iron clusters in pores in the alumina layer with increasing time at temperature. Diffusion of iron into the alumina will cause mass loss from the catalysts that grow the nanotubes, eventually causing termination of growth. Statistical analysis of the particle size distribution (Figure 1e) indicates that the morphological change of the catalyst particles is governed by two different processes, Ostwald ripening,<sup>5,20</sup> evidenced by the broadening of particle diameter distributions up to 5 min, and subsurface diffusion, evidenced by the narrowing of these distributions after 5 min. Metal cluster formation inside of the alumina layer can be attributed to the mobility of surface metal atoms combined with the long-term stability of clusters of metal atoms having bulk-like coordination in pores in the alumina. Previous spectroscopic investigations by Colaianni et al.<sup>21</sup> emphasize that subsurface diffusion of Fe into Al<sub>2</sub>O<sub>3</sub> can be initiated at temperatures as low as 600 °C. This is crucial for surface-supported catalysis since the loss of Fe from the surface to a more stable, high-coordination bulk site will lead to an irreversible change in the catalyst layer that will either severely inhibit or terminate all catalytic behavior and thus substantially impact CNT growth. In addition, recent work by Ohno et al.<sup>22</sup> has revealed the presence of Co catalyst in the subsurface layers of the alumina following growth.

To confirm that subsurface diffusion occurs during later stages of growth, we also performed cross-sectional TEM imaging following growth (with C<sub>2</sub>H<sub>2</sub>) for 30 s and 30 min to locate the Fe and understand this effect. As shown in Figure 2, after 30 min of growth, a substantial amount of Fe diffuses into the alumina, nucleating stable Fe clusters in the same manner as shown in Figure 1. To validate the presence of Fe and understand the subsurface diffusion mechanism, the crystal structures of the catalyst outlined in Figure 2 were characterized. Insets in Figure 2a and b are fast Fourier transforms (FFT, top corner) from the outlined areas and the images obtained from inverse FFT by selecting only primary diffraction spots from the FFT (bottom corner). Shown in Figure 2c is a scheme depicting features of Figure 2a and b with respect to the Fe particles and alumina layer. On the basis of the symmetry and spacing shown in FFTs and inverse FFTs (insets in Figure 2a and b), the particle on top of the Al<sub>2</sub>O<sub>3</sub> support (Figure 2a) is  $\gamma$ -phase (face-centered cubic), and the particle inside of the Al<sub>2</sub>O<sub>3</sub> support (Figure 2b) is  $\alpha$ -phase (body-centered cubic; see the Supporting Information for detailed analysis). We expect this difference to be related to the Fe particle surface coordination on the surface versus that in the bulk of the Al<sub>2</sub>O<sub>3</sub>, which drives the stability of the two different phases. This emphasizes that Fe diffusion into the oxide support occurs during growth (not just annealing) and that the bulk-like stability of clusters in the alumina support drives the atomic Fe subsurface

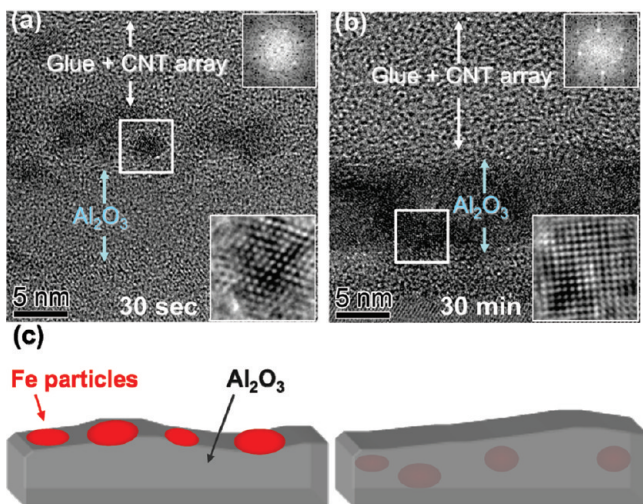


**Figure 2.** Cross-sectional TEM images of the Fe catalyst and Al<sub>2</sub>O<sub>3</sub> support following growth for (a) 30's and (b) 30 min. Insets in the top corner are the FFTs from the areas outlined in white, and insets in the bottom corner are the inverse FFTs using only the primary diffraction points from the FFTs. (c) Scheme illustrating the cross-sectional TEM images shown in (a) and (b), emphasizing the location of the Fe particles with respect to the Al<sub>2</sub>O<sub>3</sub> layer.

diffusion. In situ TEM characterization of catalyst particles under broadly analogous growth conditions was also carried out and supports the general picture emphasized in Figures 1 and 2 (see Supporting Information Figure S1 and Movie S1).

Next, to better understand the impact of catalyst morphological evolution on aligned SWNT array growth, real-time measurements of SWNT array growth rates were carried out and compared to the TEM characterization of the catalyst layers following thermal annealing. Previously, we have established that surface-mediated Ostwald ripening of the catalyst occurs regardless of the exposure to C<sub>2</sub>H<sub>2</sub>.<sup>5</sup> This enables a substantive comparison between real-time growth data and TEM characterization of annealed samples. SWNT array growth rates were monitored as a function of time using square wave pulses of C<sub>2</sub>H<sub>2</sub> to form discernible breaks<sup>23,24</sup> in the array (see the Supporting Information Figures S2–S4), allowing characterization of the growth kinetics. The thickness of the array between successive breaks was used to determine the growth rate over a well-defined time in the growth process. Utilizing this technique, a plot of the growth rate (or layer height), normalized to the first-layer growth rate, is shown in Figure 3a. Superimposed upon these data are particle number density measurements taken from TEM images (Figure 1) over a 200 × 200 nm<sup>2</sup> area. From this, three distinct regions can be identified to describe the behavior of the SWNT array growth, as further illustrated in Figure 3b. Interestingly, a striking correlation between growth behavior and the particle number density suggests that the catalyst morphological evolution plays a key role in growth termination and indeed in growth rate reduction. In accordance with Figure 1, we note that the initial retardation in growth rate (region I) is dominated by surface-mediated Ostwald ripening, and the latter retardation in growth (region III) is dominated by subsurface Fe diffusion. Region

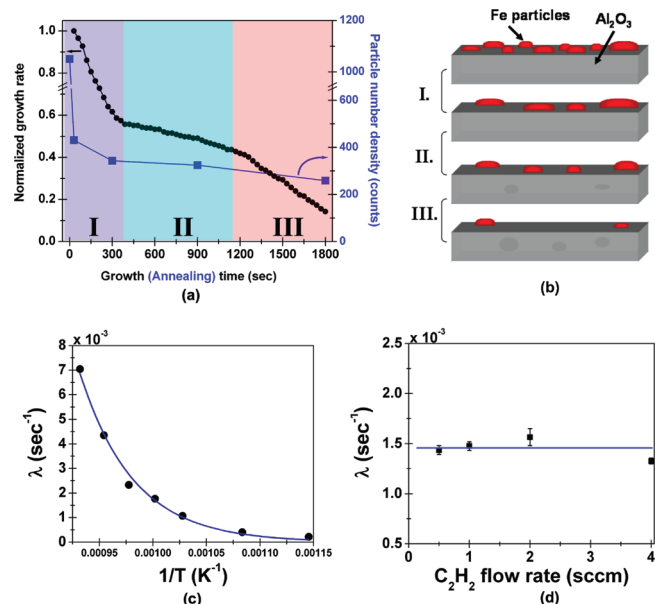


**Figure 3.** (a) Normalized growth rate from real-time growth monitoring plotted as a function of growth time. Also included on the opposing axis (blue) is the particle density from TEM characterization in Figure 1. (b) Scheme emphasizing the specific catalyst behavior in accordance with Figures 1 and 2 and how it relates to the regions of catalyst activity in the real-time growth data. Catalyst decay rate,  $\lambda$ , as a function of both the growth temperature (c) and the C<sub>2</sub>H<sub>2</sub> flow rate (equivalent to partial pressure, d).

II is interpreted as an intermediate state where the rapid planar Ostwald ripening that occurs in region I leads to stability in the catalyst particle number density due to the onset of significant 3-D subsurface diffusion. This results in an overall decrease in particle size (Figure 1e) throughout this region, but little change in particle number density. The TEM observations show that the catalyst particle number density decreases by over a factor of ~4 following 30 min of thermal annealing. Even though the SWNT array continues to grow at this point, the growth rate is substantially retarded compared to when the catalyst particle density is at maximum. We also note that a signature of termination in vertical array growth is poor alignment at the bottom of the array, as reported elsewhere.<sup>25</sup> In our experiments, we find this to be apparent following long growth (90 min–4 h), in which the decreasing number density in region III is expected to further decrease until termination takes place. We expect that the poor alignment is caused by a reduced number density of nanotubes allowing lateral freedom, which is in turn caused by a reduced number of active catalysts. Recent work by Hart's group emphasizes that growth termination occurs rapidly when the nanotube density becomes too low<sup>26</sup>, a concept that our results suggest to be influenced by Ostwald-ripening- and subsurface-diffusion-induced lowering of catalyst particle density.

Additionally, this technique for studying real-time growth also allows us to investigate the dependence of the catalyst deactivation on critical parameters. Shown in Figure 3c and d is the catalyst decay rate,  $\lambda$ ,<sup>27</sup> as a function of temperature and C<sub>2</sub>H<sub>2</sub> partial pressure, respectively. This was fit by using a decaying exponential fit to region I of curves generated

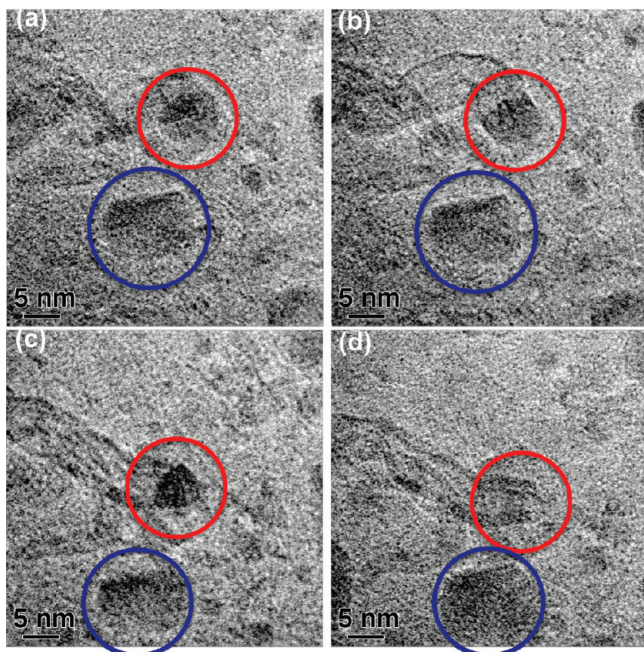


**Figure 4.** Four subsequent snapshots (a)–(d) from growth at 650 °C in 2.5 mTorr of  $\text{C}_2\text{H}_2$  and 7.5 mTorr of  $\text{H}_2$  in situ with TEM showing stages of catalyst morphological evolution and its effect in growth termination for an individual growing few-walled CNT. We note that movies of this and additional CNT and SWNT termination events are available in the Supporting Information.

similar to that shown in Figure 3a. The specific use of region I is expected to capture the kinetics of growth as the catalyst particle density exhibits the greatest change. Further information on the fitting process is described in the Supporting Information. Immediately obvious in Figure 3c and d is the strong dependence of  $\lambda$  on temperature ( $E_{\text{activation}} = 1.72 \text{ eV}$ ) but no clear dependence on  $\text{C}_2\text{H}_2$  pressure. This is consistent with the TEM analysis, emphasizing the strong temperature dependence of iron mobility (see the Supporting Information Figure S5) that is a signature of Ostwald-ripening-induced growth kinetics. This further bolsters the conclusion that catalyst morphological evolution has a significant role in growth kinetics and growth termination.

Finally, further experiments were conducted with identical catalyst layers to those utilized in Figure 3 to study growth through in situ TEM characterization. We include several videos (see the Supporting Information Movies S2 and S3) supporting the termination mechanism proposed thus far as being universal for both SWNTs and few-walled CNTs. Figure 4 shows four frames from one of these videos that captures growth, termination, and Ostwald ripening or subsequent subsurface diffusion of a catalyst particle growing a few-walled CNT. In Figure 4, one can find both (i) the disappearance of the Fe catalyst particle associated with a few-walled CNT (red circle) and (ii) the growth of an adjacent Fe particle (blue circle), both of which are clearly identified. In the final two frames, nanotube growth terminates, and the particle disappears from the base of the nanotube. This general mechanism has been observed in multiple in situ TEM experiments (for both single-walled and multiwalled

nanotubes) and is fully consistent with and supportive of the proposed mechanism for bulk termination of SWNT array growth.

In conclusion, we demonstrate here that dynamic catalyst evolution driven by thermally activated Fe surface and subsurface migration plays a fundamental role in the termination of aligned CNT array growth. Our work emphasizes a striking correlation between the catalyst particle number density measured via TEM characterization and the growth rates of the nanotube arrays. Finally, in situ TEM of the growth process validates the hypothesis that Ostwald ripening and Fe subsurface migration lower the total catalyst number density, and this subsequently causes eventual termination of a majority of growing nanotubes with time, which is a reasonable explanation for the observed termination of the overall carpet array. These insights suggest that through rational design of both the catalyst and its support, it may be possible to grow substantially longer SWNTs arrays.

**SUPPORTING INFORMATION AVAILABLE** Detailed investigation on Fe catalyst structures, in situ observation of Fe catalyst subsurface diffusion, ETEM movies for in situ growth termination and subsurface diffusion, and experimental details. This material is available free of charge via the Internet at <http://pubs.acs.org>.

## AUTHOR INFORMATION

### Corresponding Author:

\*To whom correspondence should be addressed. E-mail: eastach@ecn.purdue.edu. Tel: 765-494-1466 (E.A.S.); E-mail: Benji.Maruyama@wpafb.af.mil (B.M.).

### Author Contributions:

#These authors contributed equally.

**ACKNOWLEDGMENT** The authors thank D. Natelson for use of equipment for catalyst deposition and S. Ripley for experimental assistance. Support from AFOSR is gratefully acknowledged. C.L.P. and R.H.H. acknowledge partial support from the Lockheed Martin LANCER program. S.M.K. and E.A.S. acknowledge support from the Air Force Research Laboratory.

## REFERENCES

- (1) Hata, K.; Futaba, D. N.; Mizuno, K.; Namai, T.; Yumura, M.; Iijima, S. Water-Assisted Highly Efficient Synthesis of Impurity-Free Single-Walled Carbon Nanotubes. *Science* **2004**, *306*, 1362–1364.
- (2) Eres, G.; Kinkhabwala, A. A.; Cui, H.; Geohegan, D. B.; Puretzky, A. A.; Lowndes, D. H. Molecular Beam-Controlled Nucleation and Growth of Vertically Aligned Single-Wall Carbon Nanotube Arrays. *J. Phys. Chem. B* **2005**, *109*, 16684–16694.
- (3) Chakrabarti, S.; Nagasaka, T.; Yoshikawa, Y.; Pan, L.; Nakayama, Y. Growth of Super Long Aligned Brush-Like Carbon Nanotubes. *Jpn. J. Appl. Phys.* **2006**, *45*, L720–L722.
- (4) Pint, C. L.; Pheasant, S. T.; Parra-Vasquez, A. N. G.; Horton, C.; Xu, Y.; Hauge, R. H. Investigation of Optimal Parameters for Oxide-Assisted Growth of Vertically Aligned Single-Walled Carbon Nanotubes. *J. Phys. Chem. C* **2009**, *113*, 4125–4133.
- (5) Amama, P. B.; Pint, C. L.; McJilton, L.; Kim, S. M.; Stach, E. A.; Murray, P. T.; Hauge, R. H.; Maruyama, B. Role of Water in

- Super Growth of Single-Walled Carbon Nanotube Carpets. *Nano Lett.* **2009**, *9*, 44–49.
- (6) Christen, H. M.; Puretzky, A. A.; Cui, H.; Belay, K.; Fleming, P. H.; Geohegan, D. B.; Lowndes, D. H. Rapid Growth of Long, Vertically Aligned Carbon Nanotubes through Efficient Catalyst Optimization Using Metal Film Gradients. *Nano Lett.* **2004**, *4*, 1939–1942.
- (7) Mora, E.; Harutyunyan, A. R. Study of Single-Walled Carbon Nanotubes Growth via the Catalyst Lifetime. *J Phys. Chem. C* **2008**, *112*, 4805–4812.
- (8) Baughman, R. H.; Zakhidov, A. A.; De Heer, W. A. Carbon Nanotubes—The Route Toward Applications. *Science* **2002**, *297*, 787–792.
- (9) Hannon, J. B.; Kodambaka, S.; Ross, F. M.; Tromp, R. M. The Influence of the Surface Migration of Gold on the Growth of Silicon Nanowires. *Nature* **2006**, *440*, 69–71.
- (10) Carver, R. L.; Peng, H.; Sadana, A. K.; Nikolaev, P.; Arepalli, S.; Scott, C. D.; Billups, W. E.; Hauge, R. H.; Smalley, R. E. A Model for Nucleation and Growth of Single Wall Carbon Nanotubes Via the HiPco Process: A Catalyst Concentration Study. *J. Nanosci. Nanotechnol.* **2005**, *5*, 1035–1040.
- (11) Harutyunyan, A. R.; Mora, E.; Tokune, T.; Bolton, K.; Rosén, A.; Jiang, A.; Awasthi, N.; Curtarolo, S. Hidden Features of the Catalyst Nanoparticles Favorable for Single-Walled Carbon Nanotube Growth. *Appl. Phys. Lett.* **2007**, *90*, 163120.
- (12) Harutyunyan, A. R.; Awasthi, N.; Jiang, A.; Setyawan, W.; Mora, E.; Tokune, T.; Bolton, K.; Curtarolo, S. Reduced Carbon Solubility in Fe Nanoclusters and Implications for the Growth of Single-Walled Carbon Nanotubes. *Phys. Rev. Lett.* **2008**, *100*, 195502.
- (13) Yamada, T.; Maigne, A.; Yudasaka, M.; Mizuno, K.; Futaba, D. N.; Yumura, M.; Iijima, S.; Hata, K. Revealing the Secret of Water-Assisted Carbon Nanotube Synthesis by Microscopic Observation of the Interaction of Water on the Catalysts. *Nano Lett.* **2008**, *8*, 4288–4292.
- (14) Han, J.-H.; Graff, R. A.; Welch, B.; Marsh, C. P.; Franks, R.; Strano, M. S. A Mechanochemical Model of Growth Termination in Vertical Carbon Nanotube Forests. *ACS Nano* **2008**, *2*, 53–60.
- (15) Yoshida, H.; Shimizu, T.; Uchiyama, T.; Kohno, H.; Homma, Y.; Takeda, S. Atomic-Scale Analysis on the Role of Molybdenum in Iron-Catalyzed Carbon Nanotube Growth. *Nano Lett.* **2009**, *9*, 3810–3815.
- (16) Amama, P. B.; Pint, C. L.; Kim, S. M.; McJilton, L.; Eyink, K. G.; Stach, E. A.; Hauge, R. H.; Maruyama, B., Influence of Alumina Type on the Evolution and Activity of Alumina-Supported Fe Catalysts in Single-Walled Carbon Nanotube Carpet Growth. *ACS Nano* **2010**, doi: 10.1021/nn901700u.
- (17) Pint, C. L.; Pheasant, S. T.; Pasquali, M.; Coulter, K. E.; Schmidt, H. K.; Hauge, R. H. Synthesis of High Aspect-Ratio Carbon Nanotube “Flying Carpets” from Nanostructured Flake Substrates. *Nano Lett.* **2008**, *8*, 1879–1883.
- (18) Noda, S.; Hasegawa, K.; Sugime, H.; Kakehi, K.; Zhang, Z.; Maruyama, S.; Yamaguchi, Y. Millimeter-Thick Single-Walled Carbon Nanotube Forests: Hidden Role of Catalyst Support. *Jpn. J. Appl. Phys.* **2007**, *46*, L399–L401.
- (19) Pint, C. L.; Nicholas, N.; Duque, J. G.; Parra-Vasquez, A. N. G.; Pasquali, M.; Hauge, R. Recycling Ultrathin Catalyst Layers for Multiple Single-Walled Carbon Nanotube Array Regrowth Cycles and Selectivity in Catalyst Activation. *Chem. Mater.* **2009**, *21*, 1550–1556.
- (20) Voorhees, P. W. The Theory of Ostwald Ripening. *J. Stat. Phys.* **1985**, *38*, 231–252.
- (21) Colaianni, M. L.; Chen, P. J.; Yates, J. T., Jr. Spectroscopic Studies of the Thermal Modification of the Fe/Al<sub>2</sub>O<sub>3</sub> Interface. *Surf. Sci.* **1990**, *238*, 13–24.
- (22) Ohno, H.; Takagi, D.; Yamada, K.; Chiashi, S.; Tokura, A.; Homma, Y. Growth of Vertically Aligned Single-Walled Carbon Nanotubes on Alumina and Sapphire Substrates. *Jpn. J. Appl. Phys.* **2008**, *47*, 1956–1960.
- (23) Liu, K.; Jiang, K.; Feng, C.; Chen, Z.; Fan, S. A Growth Mark Method for Studying Growth Mechanism of Carbon Nanotube Arrays. *Carbon* **2005**, *43*, 2850–2856.
- (24) Zhu, L.; Xu, J.; Xiao, F.; Jiang, H.; Hess, D. W.; Wong, C. P. The Growth of Carbon Nanotube Stacks in the Kinetics-Controlled Regime. *Carbon* **2007**, *45*, 344–348.
- (25) Meshot, E. R.; Hart, A. J. Abrupt Self-Termination of Vertically Aligned Carbon Nanotube Growth. *Appl. Phys. Lett.* **2008**, *92*, 113107.
- (26) Bedewy, M.; Meshot, E. R.; Guo, H.; Verploegen, E. A.; Lu, W.; Hart, A. J. Collective Mechanism for the Evolution and Self-Termination of Vertically Aligned Carbon Nanotube Growth. *J. Phys. Chem. C* **2009**, *113*, 20576–20582.
- (27) Futaba, D. N.; Hata, K.; Yamada, T.; Mizuno, K.; Yumura, M.; Iijima, S. Kinetics of Water-Assisted Single-Walled Carbon Nanotube Synthesis Revealed by a Time-Evolution Analysis. *Phys. Rev. Lett.* **2005**, *95*, 056104.